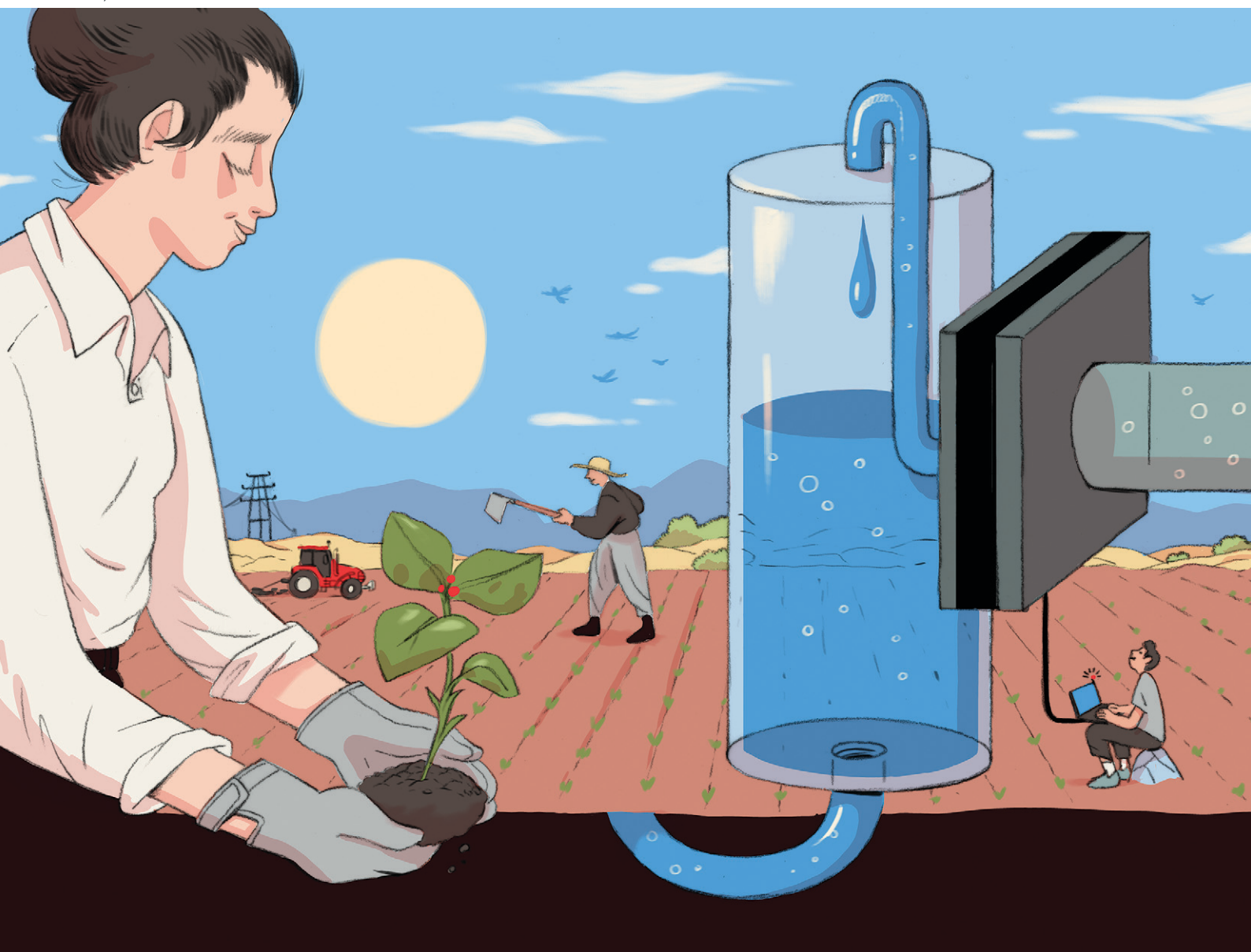


Environmental Science

Water Research & Technology

rsc.li/es-water



ISSN 2053-1400

PAPER

Matthew E. Suss *et al.*
Emerging investigator series: a comparison of strong
and weak-acid functionalized carbon electrodes in
capacitive deionization

PAPER

View Article Online
View Journal | View Issue



Cite this: *Environ. Sci.: Water Res. Technol.*, 2022, **8**, 949

Emerging investigator series: a comparison of strong and weak-acid functionalized carbon electrodes in capacitive deionization†

Rana Uwayid, ^a Charles E. Diesendruck ^{bc} and Matthew E. Suss ^{*acd}

Capacitive deionization (CDI) is a promising membraneless technology widely explored for water desalination and selective separations. The active elements in CDI are often inexpensive activated carbon electrodes, which store ions in charged micropore electric double layers. Various surface functionalizations of CDI electrodes have been explored to enhance salt storage capacity, long-term stability, and ion selectivity, including use of strong or weak-acid functional groups in CDI cathodes. However, a direct comparison of CDI performance between weak and strong-acid functionalized cathodes has not been presented. Here we fill this knowledge gap by cycle testing a single CDI cell with either a weak or strong-acid functionalized cathode for varying cycle times. We provide measurements for cell salt storage capacity and charge efficiency, as well as quantify salt capacity degradation rates. Detailed *ex situ* material characterizations yield insight into material behavior and mechanisms for electrode degradation. This data allows us to conclude that strong-acid functionalized cathodes are more pH stable and stable to charge–discharge cycling, but that current weak-acid functionalization methodologies provide cathodes with higher initial salt and charge storage capacity. Overall, the data presented here provides insights into the proper selection of surface functionalization for CDI cathodes.

Received 30th December 2021,
Accepted 21st March 2022

DOI: 10.1039/d1ew00967b

rsc.li/es-water

Water impact

Surface functionalization affects electrode stability and CDI desalination performance. Currently, the main bottleneck preventing widespread adoption of CDI in water treatment applications is electrode degradation. Our work provides insights into the proper selection of surface functionalization toward stable CDI cathodes and better performance.

Introduction

Capacitive deionization (CDI) is an emerging water treatment technology that has attracted much attention worldwide in recent years.^{1,14} In CDI, ion removal is accomplished by applying a voltage of about 1 V or current of about 1 mA cm^{−2} between a pair of electrodes, often microporous carbons, in the presence of a feedwater stream. The operation cycle consists of two steps, desalination and regeneration. When the

cell is charged, cations from the feedwater stream migrate to the cathode electric double layers (EDLs) while anions migrate to the anode EDLs. Once the charging process is complete, the electrodes are regenerated by discharging the cell. The discharge step is performed by either shorting the electrodes, modifying the applied potential window, or application of a reverse current, which releases the stored ions into a brine stream while allowing the stored energy to be recovered.^{1,2,61,62} An alternate electrosorption mechanism is *via* ion intercalation, where the ions are stored within crystallographic sites of a solid-state host compound or between atomic planes. Intercalation CDI cells utilize materials such as Prussian blue analogues (PBAs), or conversion materials such as silver or bismuth.^{4–10} Intercalation electrodes have been explored towards selective separations.^{11,12} Singh *et al.* utilized nickel hexacyanoferrate electrodes in CDI and observed high monovalent cation selectivity of Na⁺ over Ca²⁺ and Mg²⁺.¹³ Later, Singh *et al.* achieved divalent cation selectivity of Ca²⁺ over Na⁺ by utilizing the PBA vanadium

^a Faculty of Mechanical Engineering, Technion – Israel Institute of Technology, Haifa, Israel. E-mail: mesuss@me.technion.ac.il

^b Schulich Faculty of Chemistry, Technion – Israel Institute of Technology, Haifa, Israel

^c Grand Technion Energy Program, Technion – Israel Institute of Technology, Haifa, Israel

^d Wolfson Department of Chemical Engineering, Technion – Israel Institute of Technology, Haifa, Israel

† Electronic supplementary information (ESI) available. See DOI: <https://doi.org/10.1039/d1ew00967b>

hexacyanoferrate, where the substitution of nickel with vanadium switched the material from monovalent to divalent selectivity.¹¹ However, intercalation electrodes are generally more expensive than activated carbon electrodes, and not widely available at scale.^{63,64}

Surface functional groups in activated carbon micropores can strongly affect CDI cell performance. In recent years, there has been an increasing number of CDI studies that utilize functional groups as effective means to improve the salt adsorption capacity (SAC), charge efficiency, and ion selectivity.^{14–21} There are two categories of surface functionalization using acid groups: weak and strong-acid functionalization. The most common functionalization is the introduction or creation of weak acid groups *via* nitric acid oxidation,^{22–27} and amination reaction with ethylenediamine.^{28,29} Cohen *et al.* and Wu *et al.* experimentally showed that nitric acid treatment lead to functionalization of carbon micropore surfaces with carboxyl groups (COOH) which enhance SAC and charge efficiency in CDI.^{22,25} In addition, Guyes *et al.* showed that increasing COOH group concentration in cathode micropores can enhance size-based ion selectivity.³⁰ Vapnik *et al.* synthesized a redox-copolymer with carboxyl functionalization and achieved enhancement in cation-selective separations.³¹ Yang *et al.* grafted ion-selective functional groups on the surface of carbon nanotubes by amination treatments and showed a reduction in parasitic co-ion repulsion from micropores during charging.³²

Although weak-acid groups are relatively simple to add to micropores, and provide well-known performance benefits, when biased electrically such groups can undergo deleterious electron transfer reactions.³³ Uwayid *et al.* used a nitric acid-oxidized carbon cloth cathode and showed a large reduction in weak acid functional group concentration, such as COOH, during CDI cycling.³⁴ For CDI cells without chemical functionalization, it has been well-characterized that anode electro-oxidation is the major salt capacity degradation mechanism.^{35–38} Contrarily, for cells with oxidized cathodes the anode's effect on cell degradation is minimal, and the cathode plays a major role due in part to loss of carboxyl functional groups during cycling. Further, since carboxyl groups have a pK_a of ≈ 4 –5, the micropore chemical charge concentration can be strongly affected by the local solution pH.³⁴

Overall, CDI literature to date has tended to focus on weak-acid functionalization of CDI electrode surfaces, with far less attention being paid to the effect of strong-acid functional groups. Yet, attachment of strongly acidic sulfonic groups ($-\text{SO}_3\text{H}$) to micropores have shown an enhancement in CDI performance relative to cells with pristine carbon cathodes.^{39–43} Being hydrophilic in nature, $-\text{SO}_3\text{H}$ is expected to improve the wettability of carbon materials as previously shown in various works.^{40,44,45} Further, as $-\text{SO}_3\text{H}$ typically has a $pK_a \approx -3$ in water, the chemical charge concentration in the micropores is expected to be largely pH independent even in very acidic water.¹⁶ Niu *et al.* treated activated carbon electrodes with sulfuric acid using a hydrothermal protocol, leading to an enhancement in attained charge efficiency and salt

adsorption compared to untreated activated carbon.³⁹ Similarly, Ho Min *et al.* showed an improvement in both the specific adsorption capacity and the charging efficiency after sulfonation of a commercially activated carbon/titania hybrid electrode.⁴⁶ Park *et al.* successfully performed the surface modification of activated carbon (AC) granules for a flow electrode CDI system with ammonium and sulfonic groups using an emulsion polymerization method. The modified AC induced electrostatic repulsion, which decreased the viscosity of the suspension and the salt removal efficiencies were improved from 8.2% to 27.7%.⁴¹ Recently, Daripa *et al.* used ammonium sulfate on graphene oxide for an electrochemical supercapacitor and obtained a higher electrode capacitance and enhanced the electrocatalytic activity.⁴² Ma *et al.* used sulfonated carbon nanotubes (CNT) as a cathode and untreated CNT as anode and observed wettability and ion selectivity enhancement.⁴⁵ However, the latter author observed a SAC reduction of 12.0% after 10-cycles with applying voltage of 1.2 V. This reduction was attributed to the decline of the anodic potential of zero charge (E_{pzc}) after cyclic adsorption/desorption, indicating that degradation occurred mainly at the anode surface while sulfonated surface was more stable.⁴⁵ Increasing the anode-to-cathode mass ratio improved anode stability.⁴⁷ Sulfonated cathodes have also been shown to enhance ion selectivity in CDI. Guyes *et al.*, used a sulfonated activated carbon cathode and found that such treatment enhanced the monovalent cation selectivity of Na^+ over Ca^{2+} .¹⁵ Uwayid *et al.* showed that using sulfonated carbon cloth cathode enabled perfect divalent cation selectivity of Ca^{2+} over Na^+ .¹⁷

Here we directly compare for the first time, to the best of our knowledge, the performance and stability of a CDI cell with strong-acid (sulfonic) functional groups in cathode micropores to one with weak-acid functional groups. Such comparisons are done using 100-cycle CDI experiments with constant voltage operation, and *ex situ* cathode characterizations pre and post cycling experiments. Our data shows that the weak-acid functionalized cathode presented higher initial SAC, but that use of sulfonated cathodes can reduce cell degradation rates over long-term operation for long full cycle times (FCT). We further elucidate degradation mechanisms for sulfonated cathodes, which appear to be largely due to production of weak-base groups in micropores and not loss of sulfonic groups.

Experimental

Materials and methods

Electrode material. The as-received electrode material used in this work was made of commercial activated carbon cloth (ACC-5092-15, ~ 500 μm thickness, Kynol Europa GmbH, Germany), with specific micropore volume 0.68 $\text{cm}^3 \text{g}^{-1}$ based on nitrogen gas sorption analysis.³⁴ The carbon cloth was first cut into 2.5×2.5 cm^2 electrodes, rinsed with deionized (DI) water (18.2 M Ω , Synergy Water Purification System, Merck Millipore KGaA), and then dried in air at

80 °C for 3 h. The washed, untreated samples are referred to as pristine electrodes.

Sulfonation and oxidation pretreatments

For electrode oxidation, to enhance the micropore concentration of weak-acid groups, ~0.8 gr of washed commercial activated carbon cloth was soaked in 50 mL of 70% nitric acid (HNO_3) at room temperature for 24 h. Then, it was immersed in 800 mL of DI water for 12 h. The water was replaced with a fresh, equal volume of DI water three times, each time for 30 min, at the end of which the pH at the carbon surface was measured to be ~7.³⁴

For sulfonation to make electrodes with strong-acid groups, unwashed commercial activated carbon cloth was soaked in 20% fuming sulfuric acid ($\text{H}_2\text{SO}_4\text{-SO}_3$) and kept 24 h at room temperature (volume to mass ratio >7 mL g^{-1}). Then, the liquid was poured out and the material was soaked in 50 mL of hexane for 15 min while keeping the material raised in the beaker to let the remaining H_2SO_4 sink to the bottom and be separated from the electrode as much as possible. Finally, the material was immersed in ~500 mL ice for 30 min and then soaked with 200 mL DI water three times (30 min each). The electrodes were then dried in an oven at 60 °C overnight.¹⁵

CDI cell structure. The CDI cell used a flow-through electrodes (FTE) architecture in which the feed stream flows directly through the electrode macropores, as described in Fig. 1a. The cell consists of two impervious graphite current collectors to make electrical contact with the electrodes (FC-GR, Graphitstore.com, Inc., Buffalo Grove, IL, USA), four expanded PTFE gaskets to seal the cell (W. L. Gore & Associates, Gore-Tex NSG16X-GP, 1.4 mm uncompressed thickness, $5 \times 5 \text{ cm}^2$), and a porous separator to electrically isolate the cathode and anode (GE Life Science, Whatman Grade 2 cellulose filter paper, 190 μm thickness). The upstream electrode is the

cathode, and the downstream is the anode. The micropore of the functionalized cathode used in this work is shown schematically in Fig. 1b for the weak-acid functionalization and 1c for the strong-acid functionalization. Feed water flows through an array of milled cylindrical channels in the current collectors, each of 1.5 mm diameter and 3 mm length, and between the fibers in the electrodes. The current collectors are connected to the negative and positive terminals of a voltage source (2400 Source Meter, Keithley Instruments, Langley, Berkshire, England). The cell terminates with PVDF endplate upstream and ABS endplate downstream.

CDI experiments. The feed solution used for all experiments was 20 mM NaCl in DI water. Dissolved oxygen in the feedwater can enhance CDI cell degradation rates during cycling,^{36,48,49} thus, prior to CDI experiments, the solution was sparged with nitrogen gas for 3 h until the dissolved oxygen reached ~2.5% saturation (Orion Star A213, Thermo Fisher Scientific, USA). A peristaltic pump (Masterflex 0755130, Cole Parmer, USA) supplied the feed solution into the CDI cell from a tank at a flow rate of 1 mL min^{-1} . Single-pass experiments of 100 charge–discharge cycles for various full cycle times (FCT) were carried out at a constant voltage of 1 V under continuous N_2 sparging of the feed. The cell was discharged at 0 V. The effluent conductivity was measured using a flow-through conductivity sensor (Tracedec 390-50, Innovative Sensor Technologies GmbH, Austria). Each experiment was repeated three times to confirm repeatability, with representative results provided here. The cell tested with a pristine anode and sulfonated cathode is referred to as sulfonated-pristine (SP) cell, and with an oxidized cathode and pristine anode is referred to as oxidized-pristine (OP) cell.

Electrode material characterization

The electrode morphology and surface chemistry were characterized with direct titrations, nitrogen gas sorption, and elemental analysis. The micropore volume of a given electrode material was determined from N_2 adsorption–desorption isotherms (3Flex Physisorption, Micromeritics, USA). The samples were degassed in vacuum at 200 °C for 10 h and the measurement was carried out at 77 K. The Brunauer–Emmet–Teller (BET) model is utilized to calculate the specific surface area.

For the elemental analysis of pre- and post-experiment electrodes, the materials were dried under ultra-high vacuum then induced coupled plasma (ICP) measurements were performed to quantify the elements' concentration in the materials (Thermo-Scientific iCAP 6000 ICP-OES analyzer, MIKROLAP, Germany). Fourier-transform infrared spectroscopy (FTIR) (Tensor 27, Bruker Optik GmbH, Germany) was utilized for determination of the chemical bonds present at the surface after oxidation and sulfonation treatment compared to pristine. 1 mg of material was mixed with 200 mg KBr in a mortar while grinding with the pestle. The mixture was added in the pellet die and pressed. The formed pressed disc was used in FTIR with attenuated total reflectance (ATR) mode.

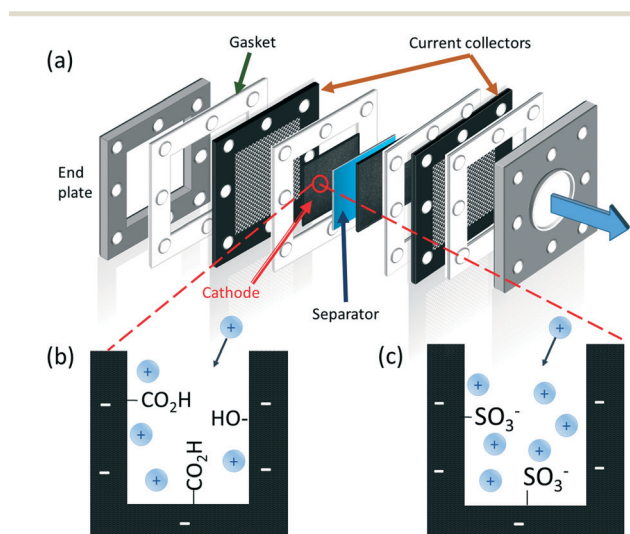


Fig. 1 Schematic structure of (a) CDI cell (b) weak-acid functionalized cathode micropores containing $-\text{COOH}$ and $-\text{OH}$ groups, and (c) strong-acid functionalized cathode containing $-\text{SO}_3^-$ groups.

Scanning electron microscopy (SEM) imaging was performed on a high-resolution scanning electron microscope equipped with a Schottky field-emission electron gun and a Gemini electron-beam column design (Zeiss Ultra Plus, Germany). To prevent charging and capture nanometric size features in the investigated system, the microscope was operated in a low voltage mode around 1 keV electron beam energy. Images were acquired by a high-resolution In-the-Lens secondary electrons (SE) detector, at a working distance of about 3 mm.

For pre-experiment titrations, ~0.4 g of electrode material was pulverized using a mortar and pestle. Then the powder was immersed in a 0.011 M NaOH solution and sparged with N₂ gas for 40 min. The solution was stirred constantly for 24 h, transferred to a 150 ml vessel in an automated titrator (Titrand 904 and iAquatrode Plus Pt1000, Metrohm AG, Switzerland), and sparged with gaseous N₂ for an additional 20 min before the analysis was initiated. The solution was titrated by adding 10 μ L droplets of 0.05 M HCl under continuous N₂ sparging, and dwelling after each droplet until attaining steady solution pH (potential drift of <0.5 mV min⁻¹). The aforementioned procedure was also used to titrate a blank solution (without electrode material) as a control. For post-experiment titrations, the material was soaked in 1 M HCl for 24 h to exchange sodium ions with protons as counterions to the sulfonic groups. Then, it was soaked in DI water to remove the excess acid until the pH reached ~7 followed by the same pre-experiment titration procedure. Each titration was repeated three times to confirm repeatability, with representative results provided here.

Results and discussion

Pre-experiment material characterizations

For quantification of the chemical charge concentration in electrode micropores, direct titrations of unused electrodes were performed. Fig. 2a shows the result of direct titration of blank solution containing no carbon, and for solution containing as-received (pristine), oxidized (weak acid), or

sulfonated (strong acid) materials, as measured solution pH *versus* titrant volume added. As can be seen in Fig. 2a, the pristine curve is very similar to the blank curve, indicating that pristine material includes only a small amount of acidic groups. While both the pristine and blank curves begin at pH = 12 for $V = 0$ mL, the oxidized and sulfonated curves begin at pH between 11.4–11.6, and the latter curves are shifted to the left relative to blank and pristine curves. This is attributed to a substantial increase in the amount of micropore acid functional groups after treatment, as expected from previous works employing nitric acid and sulfonation pretreatment.^{15,29,30,50} The titration curve of the oxidized carbon presents a more gradual shift in pH with increasing titrant volume, characteristic of the titration of weak acid groups, as opposed to the sulfonated curve which has a much sharper shift in pH.

Fig. 2b shows the net micropore chemical surface charge concentration, σ_{chem} , of pristine, oxidized, and sulfonated materials *versus* solution pH. This was obtained from fitting the titration data of Fig. 2a to the electrode titration model of Guyes *et al.*³⁰ but with an additional strong-acid term (ESI† section 2). As can be seen in Fig. 2b, at pH 7, the net micropore chemical charge concentrations of the pristine and oxidized materials are calculated to be -0.07 M and -1.5 M, respectively. These results support the fact that the pristine material contains insignificant weak-acid group concentration in the micropores while nitric-acid treatment significantly raises the concentration of weak-acid functional groups. Elemental analysis indicates a significant increase in oxygen content after oxidation (Table 1), as also shown previously, which taken together with the titration results suggest a large population of COOH functional groups in micropores.³⁴ Notably, σ_{chem} for the sulfonated material is approximately constant in the pH range of 2–6 at ~-1.3 M, characteristic of strong acid group behaviour. Guyes *et al.* presented nearly the same σ_{chem} value for a pre-experiment sulfonated electrode, at -1.2 M.¹⁵ Further, the elemental analysis shows an increase in sulfur content after sulfonation up to 0.69% compared to <0.01% for the pristine material (Table 1). As can be seen in Fig. 2b, at pH > 7, the net chemical charge concentration for the oxidized material is higher than the

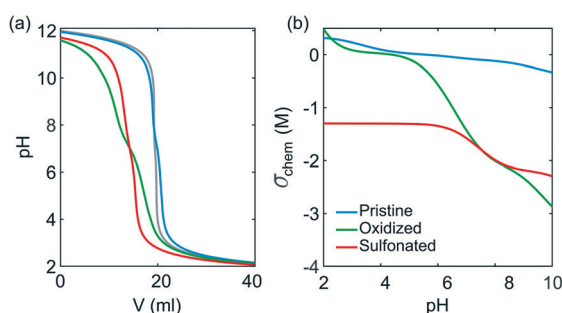


Fig. 2 (a) Results of direct titration measurements for pristine, oxidized and sulfonated microporous carbons, take pre-CDI experiments. Also shown is the titration of a blank solution with no carbon (grey line). (b) Chemical surface charge concentration, σ_{chem} , vs. pH of pristine, oxidized and sulfonated materials, obtained from EDL model to titration data fitting.

Table 1 Elemental analysis in weight % of various electrodes pre- and post-CDI cycling, measured by inductively coupled plasma mass spectrometry (ICP-MS)

		FCT (min)	C	O	S	H	N
Pristine	Unused	—	95.10	1.76	<0.01	1.11	1.44
Oxidized material	Pre-exp.	—	88.3	7.96	<0.01	0.89	2.18
	Post-exp.	100	85.09	4.51	<0.01	1.65	1.66
		30	86.87	5.99	<0.01	0.98	1.87
		10	86.4	6.89	<0.02	1.16	2.04
Sulfonated material	Pre-exp.	—	92.70	2.11	0.69	0.98	1.00
	Post-exp.	100	94.24	1.92	0.42	0.89	1.03
		30	93.87	2.09	0.44	1.01	1.05
		10	93.08	2.16	0.55	0.96	1.03

sulfonated electrode. This can be explained by the presence of significant amount of OH groups in the oxidized material relative to sulfonated material. Overall, these results show that materials based on strong-acid functional groups can be expected to show more pH-independent surface charge, especially at acidic solutions. This can be beneficial in CDI cells when needed in applications where a highly negative chemical charge is required within the acidic environment of the anode, as in inverted CDI (i-CDI) for example.^{28,35}

The sulfur atom can be affixed to carbon surfaces by interaction with oxygen-containing functional groups or by direct addition to unsaturated sites.^{51,52} Several sulfur-containing functional main groups can be present on a carbon surface modified with fuming sulfuric acid, as shown by Terzyk.⁵³ Reduced sulfur groups such as thiols (–SH), thioethers (C–S–C) and others, can be present if the carbon material is sourced from products with contained sulfur originally. However, this is not the case here, as our ICP results indicated, the pristine carbon had no sulfur content (Table 1). Sulfonic acids (RSO₃–H) are obtained from direct sulfonation of aromatics, but in addition, organosulfates (RSO₄H) can be obtained when sulfonation occurs on surface alcohol groups. To gather further insight on the type of functional groups present in the sulfonated material in this work, FTIR was performed (ESI† section 1.2). The measured transmission FTIR spectra of the sulfonated electrode material shows distinctive multiple peaks at a wavenumber range 1030–1260 cm^{–1}, which can be assigned to the vibration bands of S=O symmetric and asymmetric stretching, present in sulfonic groups. This is further evidence to support the presence of sulfonic functional groups on the electrode surface, with similar FTIR results shown in Gueyes *et al.*¹⁵ For the activated carbon material, the band at wavenumber 1630 cm^{–1} is assigned to the aromatic C=C stretching.⁵⁴ The intense broad envelope centered at wavenumber 3425 cm^{–1} is assigned to the O–H stretching modes present in COOH and phenolic groups in the sulfonated and oxidized material.^{22,33} Similar peaks were also detected for sulfonated CNT by Ma *et al.*⁴⁵ For the oxidized material, a peak appears at a wavenumber of 1730 cm^{–1}, indicating the presence of C=O bonds.

SEM images shows that the woven fibers of the pristine material are ~18 μm in diameter, and contain <1 μm hole-type features along the fiber, with similar features for the sulfonated material. Similarly, Ma *et al.* observed that sulfonation treatment did not change the observable CNT features.⁴⁵ Meanwhile, oxidation leads to a visibly smoother fiber texture, as also shown by Uwayid *et al.*³⁴ Such SEM images cannot resolve smaller features such as the micropores along the fibers. Based on nitrogen (N₂) adsorption analysis, the specific micropore volume of pristine, oxidized, and sulfonated materials are 0.55, 0.52, and 0.55 cm³ g^{–1}, respectively (ESI† section 1.1, Table S1). Thus, oxidation pre-treatment causes a 5.5% reduction in micropore volume. Molina-Sabio *et al.* showed a slight reduction in micropore volume, less than 2%, after nitric acid treatment.⁵⁵ Gao *et al.* and Wu *et al.* reported a higher reduction in micropore vol-

ume after nitric acid treatment with 12.2% and 13.5%, respectively.^{22,29} Molina-Sabio *et al.* and Shim *et al.*, related the reduction in micropore volume to the increase of oxygen-containing functional groups after oxidation, which they speculated could block some micropores.^{55,56} However, Macías-García *et al.*, treated activated carbon with nitric acid and investigated a slight increase in micropore volume.⁵⁷ Unlike oxidation, our results here suggest sulfonation pre-treatment did not significantly affect micropore volume.

CDI experiments

To compare the performance of weak-acid and strong-acid functionalized cathodes on desalination by CDI, we performed a 100-cycle experiment using a CDI cell with a pristine anode and functionalized cathode, and a 20 mM NaCl feed. The data shown in the figures are from the limit cycle, the cycle at which the conductivity profile reaches a dynamic steady state, which in our case is typically the third cycle.³ The cell with sulfonated cathode is referred to as the SP cell, and with nitric acid-oxidized cathode as the OP cell. Fig. 3 shows the results for varying full cycle time (FCT), including measured SAC, charge stored (*q*) charge efficiency (λ_{cycle}) and coulombic efficiency (CE) with either a sulfonated or nitric acid-oxidized cathode. In Fig. 3a, at FCT 100 min (charging for 50 min), it can be seen that the OP cell (black filled circles) demonstrates a SAC of 16.2 mg g^{–1} at the limit cycle, compared to 13.4 mg g^{–1} for SP cell (red circles). Overall, both treated cathodes show higher SAC values compared to an identical cell with a pristine cathode, which showed a limit cycle SAC of 8.7 mg g^{–1} under the test same conditions, as reported in Uwayid *et al.*³⁴

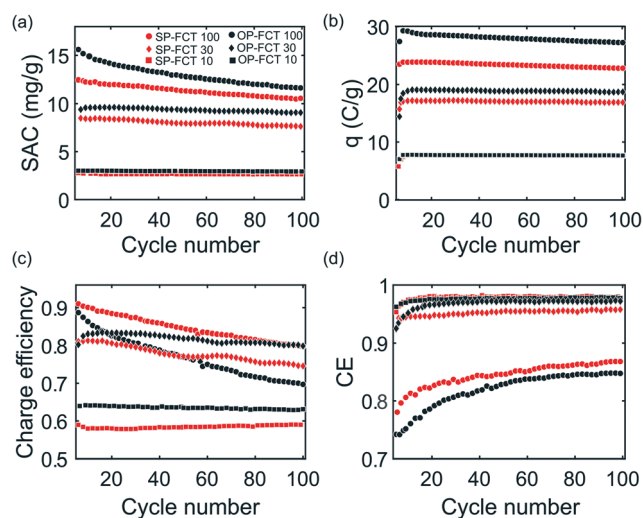


Fig. 3 Measured CDI cell performance with varying full cycle times (FCT, 100, 30, and 10 min), including: a) salt adsorption capacity (SAC), b) charged stored (*q*), c) charge efficiency (λ_{cycle}), and d) coulombic efficiency (CE) of both a sulfonated-pristine (SP) and oxidized-pristine (OP) cell versus cycle number. The feed was 20 mM NaCl, the voltage during charging was 1 V, and during discharging 0 V.

The higher limit cycle SAC achieved for the OP cell may be partially due to higher micropore chemical charge and surface area for the oxidized cathode relative to the sulfonated cathode (ESI† document, Table S1). Holubowitch *et al.* showed that CDI cathode pH can reach up to ~ 9 – 10 , and as can be seen in Fig. 2, at pH = 10, the net chemical charge value for oxidized cathode is more negative at $\sigma_{\text{chem}} = -2.8$ M than sulfonated $\sigma_{\text{chem}} = -2.4$ M.⁵⁸ We observe that by the 100th cycle, SAC values for the OP cell and SP cell at FCT 100 min are 11.3 mg g^{-1} and 10.5 mg g^{-1} , respectively. Thus, the cell with nitric acid-oxidized cathode salt storage was reduced by $\sim 30\%$,³⁴ while the cell with sulfonated cathode degraded by $\sim 21\%$, which can be compared to 48% degradation for a cell with a pristine cathode, as shown by Uwayid *et al.*³⁴ To our knowledge, this is one of very the few reports of CDI cell cycle testing with sulfonated electrodes. Ma *et al.* ran 10-cycles CDI experiment at voltage of 1.2 V using sulfonated CNTs as cathode and untreated CNTs as anode and observed a 12.0% reduction in SAC.⁴⁵ Recently, Guyes *et al.* performed 1000-cycle CDI experiment using sulfonated activated carbon cathode at a charging voltage of 1.2 V and 6 min FCT, and achieved highly-stable electrodes performance with coulombic efficiency $>96\%$.¹⁵

As can be seen in Fig. 3a, if FCT is reduced to 30 min (charging for 15 min), SAC was 9.5 mg g^{-1} and 8.5 mg g^{-1} for the OP (black diamond) and SP (red diamond) cells at the limit cycle, respectively. By the 100th cycle, OP cell salt storage was reduced by 9.3%, while the SP cell by 5.9%. Further reducing of FCT to 10 min (5 min charging) leads to smaller difference in SAC values, 3 mg g^{-1} and 2.8 mg g^{-1} for OP (black squares) and SP (red squares) cells, respectively, with capacity reduction of less than 1% for both cells over 100 cycles.

In Fig. 3b, it can be seen that the SP cell has lower charge stored per gram of material, 23.8 C g^{-1} at 100 min FCT, as compared to OP cell at 29.2 C g^{-1} at 100 min FCT. The enhanced charge storage for the OP cell is seemingly the main factor underlying its higher salt storage capacity relative to the SP cell (Fig. 2a). Charge stored degraded slightly for both cells when cycling at 100 min FCT, by 6.8% (to 27.2 C g^{-1}) and 4.2% (22.8 C g^{-1}) for the OP and SP cells, respectively. As FCT decreased, the electrodes were no longer fully charged before discharging, and so the charge stored per cycle decreases. At 10 min FCT both cells have about the same amount of charge stored per gram material of $\sim 7.8 \text{ C g}^{-1}$. As shown in Fig. 3c, the SP cell has a higher charge efficiency (λ_{cycle}) at the limit cycle of 0.95 compared to 0.91 for the OP cell (100 min FCT), which suggests reduced co-ion expulsion for the SP cell relative to the OP cell. However, at lower FCT, λ_{cycle} for the OP cell is higher than that of the SP cell. For example, at 10 min FCT λ_{cycle} equals 0.64 for the OP cell and 0.58 for the SP cell. Fig. 3d shows the coulombic efficiency (CE) versus cycle number which is used as an indicator of the prevalence of deleterious side-reactions during charging. In the initial cycles, the carbon is more reactive and so CE is relatively low,

rising sharply with cycle number. After several cycles, CE reaches an asymptotic value and remains nearly constant for the rest of the experiment.⁵⁹ The CE of the SP cell at 100 min FCT reaches about 0.84 by the 100th cycle compared to 0.82 for OP cell. Meanwhile, for FCT of 30 min and 10 min, CE reached above 0.9 for both cells, and up to 0.96.

Overall, while both cells degrade during cycling as evidenced by a reduced salt storage capacity, the SP cell degrades at a somewhat reduced rate. The degradation of the OP cell was previously studied in detail by Uwayid *et al.*,³⁴ and this was attributed to both micropore volume reduction and weak acid group loss at the cathode during cycling. Fig. 4a shows measured σ_{chem} of oxidized and sulfonated materials, now including data from direct titrations performed post-CDI cycling experiment using 100 min FCT. As can be seen in Fig. 4a, σ_{chem} of both materials shift to more positive values post experiment for all pH values tested. For example, at pH = 7, σ_{chem} of the oxidized material decreases from -1.6 to -0.25 M while σ_{chem} of sulfonated carbon decreases from -1.8 to -0.7 M.

To probe the mechanistic reason for such reduction in the magnitude of net chemical charge of the sulfonated material, Fig. 4b shows results from the fitted micropore EDL model (ESI† document, section 2). We plot the total deprotonated micropore acid concentration (including both strong and weak acids), C_A , and protonated weak base concentration, C_B , for pre- and post-experiment sulfonated material. As can be seen in Fig. 4b, in the 2–5 pH range, there is no significant change in the micropore strong acid (sulfonic group) concentration due to CDI cycling, as it remains at ~ 2.6 M both pre- and post- experiment. Meanwhile, the basic group concentration increases significantly from 1.3 M before the experiment to 2.4 M after cycling. This explains the reduction in the magnitude of net micropore chemical charge of the sulfonated material, as seen in Fig. 4a, which attains only ~ -0.3 M in the pH range 2–5 after CDI cycling. This suggests that the

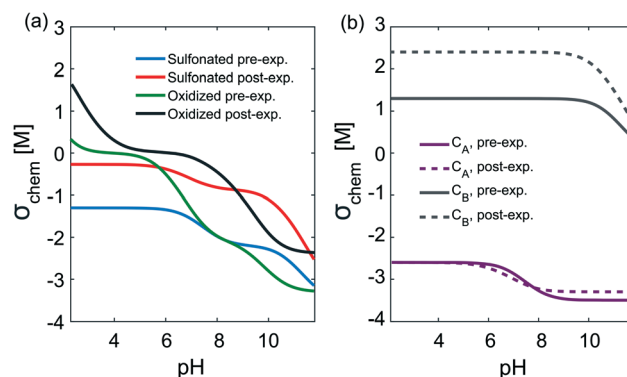


Fig. 4 a) Net micropore chemical charge concentration, σ_{chem} , of pre- and post-experiment sulfonated and oxidized materials versus pH, obtained from model-to-titration data fitting.³⁰ b) The micropore concentration of deprotonated acidic groups, C_A , and protonated basic groups, C_B , for pre- and post-experiment sulfonated material.

sulfonic groups are mostly stable during CDI cell cycling, but rather the production of weak base groups is mainly responsible for the degradation of salt storage for the SP cell. The chemical nature of the base groups is not clear, but will be explored in a future work.

The elemental analysis results are summarized in Table 1, providing additional insight as to the effects of CDI cycling on the oxidized and sulfonated cathodes. As can be seen, CDI cycling leads to a decrease in oxygen content (in weight %) for the oxidized cathode material from 7.96 to 4.51% for 100 cycles at 100 min FCT, consistent with a significant loss of carboxyl groups (Fig. 4a).³⁴ Meanwhile only a small reduction in oxygen content is observed for the sulfonated material after cycling. However, for the sulfonated cathode, there is a reduction in sulfur content from 0.69% pre-experiment to 0.55, 0.44, and 0.42% for post-experiment material with FCT 10, 30, and 100 min, respectively. As our titration results indicate no significant loss of sulfonic groups upon cycling, and Table 1 shows that loss in oxygen content was small, the loss in sulfur atoms detected by elemental analysis may be largely a loss of electrochemically inactive sulfur, for example from functional groups electrically isolated from the graphitic material or connected through non-acidic functionalities such as sulfonic esters.^{33,60}

Conclusions

We directly compared the performance of a CDI cell when using an oxidized cathode with weak-acid functional groups, and when using a sulfonated cathode with strong-acid functional groups. We showed that the cell with oxidized cathode enabled higher initial cycle salt absorption capacity, but also presented a higher degradation rate of this capacity with cycle number. We further collected titration and elemental analysis data which elucidated that the degradation of the sulfonated material during cycling is due to the formation of basic groups in cathode micropores, with loss in sulfur content likely due to the loss of inactive sulfur. Overall, due to good pH-stability and cycling stability, strong-acid functionalized cathodes are highly promising for CDI. Future work will focus on identifying the weak base groups formed during cycling on the sulfonated cathode, attempt to mitigate their formation, and optimize the sulfonation protocol to further enhance micropore chemical charge concentration.

Author contributions

Rana Uwayid: investigation, data curation, formal analysis, writing – original draft. Charles E. Diesendruck: supervision, writing – review & editing. Matthew E. Suss: conceptualization, supervision, writing – review & editing.

Conflicts of interest

There are no conflicts to declare.

Acknowledgements

This work was supported by the Israel-U.S. Collaborative Water-Energy Research Center (CoWERC), via the Binational Industrial Research and Development Foundation (BIRD) Energy Center grant EC-15. Nitrogen adsorption measurements and analysis were carried out by Mr. Eliyahu Farber. SEM micrographs were taken by Dr. Olga Kleinerman at Electron Microscopy Center, Technion, Israel. ICP analysis carried out by Mikroanalytisches Labor Kolb (MIKROLAB), Osterfelder, Germany. Rana Uwayid would like to acknowledge the support of the Arian de Rothschild women doctoral program.

Notes and references

- 1 M. E. Suss, S. Porada, X. Sun, P. M. Biesheuvel, J. Yoon and V. Presser, *Energy Environ. Sci.*, 2015, **8**, 2296–2319.
- 2 Y. Oren, *Desalination*, 2008, **228**, 10–29.
- 3 S. Porada, R. Zhao, A. Van Der Wal, V. Presser and P. M. Biesheuvel, *Prog. Mater. Sci.*, 2013, **58**, 1388–1442.
- 4 K. Singh, S. Porada, H. D. de Gier, P. M. Biesheuvel and L. C. P. M. de Smet, *Desalination*, 2019, **455**, 115–134.
- 5 J. Chang, F. Duan, C. Su, Y. Li and H. Cao, *Environ. Sci.: Water Res. Technol.*, 2020, **6**, 373–382.
- 6 S. Kim, J. Lee, C. Kim and J. Yoon, *Electrochim. Acta*, 2016, **203**, 265–271.
- 7 S. Porada, A. Shrivastava, P. Bukowska, P. M. Biesheuvel and K. C. Smith, *Electrochim. Acta*, 2017, **255**, 369–378.
- 8 P. Srimuk, F. Kaasik, B. Krüner, A. Tolosa, S. Fleischmann, N. Jäckel, M. C. Tekeli, M. Aslan, M. E. Suss and V. Presser, *J. Mater. Chem. A*, 2016, **4**, 18265–18271.
- 9 F. Xing, T. Li, J. Li, H. Zhu, N. Wang and X. Cao, *Nano Energy*, 2017, **31**, 590–595.
- 10 P. Srimuk, J. Lee, S. Fleischmann, M. Zeiger, C. Kim, M. Aslan and V. Presser, *J. Mater. Chem. A*, 2017, **5**, 15640–15649.
- 11 K. Singh, G. Li, J. Lee, H. Zuilhof, B. L. Mehdi, R. L. Zornitta and L. C. P. M. de Smet, *Adv. Funct. Mater.*, 2021, **31**, 2105203.
- 12 J. Kim, A. Jain, K. Zuo, R. Verduzco, S. Walker, M. Elimelech, Z. Zhang, X. Zhang and Q. Li, *Water Res.*, 2019, **160**, 445–453.
- 13 K. Singh, Z. Qian, P. M. Biesheuvel, H. Zuilhof, S. Porada and L. C. P. M. de Smet, *Desalination*, 2020, **481**, 114346.
- 14 J. G. Gamaethiralalage, K. Singh, S. Sahin, J. Yoon, M. Elimelech, M. E. Suss, P. Liang, P. M. Biesheuvel, R. L. Zornitta and L. C. P. M. De Smet, *Energy Environ. Sci.*, 2021, **14**, 1095–1120.
- 15 E. N. Guyes, A. N. Shocron, Y. Chen, C. E. Diesendruck and M. E. Suss, *npj Clean Water*, 2021, **4**, 1–11.
- 16 Y. Cheng, Z. Hao, C. Hao, Y. Deng, X. Li, K. Li and Y. Zhao, *RSC Adv.*, 2019, **9**, 24401–24419.
- 17 R. Uwayid, E. N. Guyes, A. Shocron, J. Gilron, M. Elimelech and M. E. Suss, *Water Res.*, 2021, **210**, 117959.
- 18 Q. Dong, X. Guo, X. Huang, L. Liu, R. Tallon, B. Taylor and J. Chen, *Chem. Eng. J.*, 2019, **361**, 1535–1542.

- 19 D. I. Oyarzun, A. Hemmatifar, J. W. Palko, M. Stadermann and J. G. Santiago, *Water Res.: X*, 2018, **1**, 100008.
- 20 X. Su and T. A. Hatton, *Phys. Chem. Chem. Phys.*, 2017, **19**, 23570–23584.
- 21 R. Chen, T. Sheehan, J. L. Ng, M. Brucks and X. Su, *Environ. Sci.: Water Res. Technol.*, 2020, **6**, 258–282.
- 22 T. Wu, G. Wang, Q. Dong, B. Qian, Y. Meng and J. Qiu, *Electrochim. Acta*, 2015, **176**, 426–433.
- 23 W. Huang, Y. Zhang, S. Bao, R. Cruz and S. Song, *Desalination*, 2014, **340**, 67–72.
- 24 S. Bao, J. Duan and Y. Zhang, *Chem. Eng. Technol.*, 2018, **41**, 1793–1799.
- 25 I. Cohen, E. Avraham, M. Noked, A. Soffer and D. Aurbach, *J. Phys. Chem. C*, 2011, **115**, 19856–19863.
- 26 L. Han, K. G. Karthikeyan, M. A. Anderson and K. B. Gregory, *J. Colloid Interface Sci.*, 2014, **430**, 93–99.
- 27 O. Sufiani, H. Tanaka, K. Teshima, R. L. Machunda and Y. A. C. Jande, *Sep. Purif. Technol.*, 2020, **247**, 116998.
- 28 X. Gao, A. Omosebi, J. Landon and K. Liu, *Environ. Sci. Technol.*, 2015, **49**, 10920–10926.
- 29 X. Gao, S. Porada, A. Omosebi, K. L. Liu, P. M. Biesheuvel and J. Landon, *Water Res.*, 2016, **92**, 275–282.
- 30 E. N. Guyes, T. Malka and M. E. Suss, *Environ. Sci. Technol.*, 2019, **53**, 8447–8454.
- 31 H. Vapnik, J. Elbert and X. Su, *J. Mater. Chem. A*, 2021, **9**, 20068–20077.
- 32 J. Yang, L. Zou and N. R. Choudhury, *Electrochim. Acta*, 2013, **91**, 11–19.
- 33 T. J. Bandoz and C. O. Ania, *Interface Sci. Technol.*, 2006, **7**, 159–229.
- 34 R. Uwayid, N. M. Seraphim, E. N. Guyes, D. Eisenberg and M. E. Suss, *Carbon*, 2021, **173**, 1105–1114.
- 35 X. Gao, A. Omosebi, J. Landon and K. Liu, *J. Phys. Chem. C*, 2018, **122**, 1158–1168.
- 36 Y. Bouhadana, E. Avraham, M. Noked, M. Ben-Tzion, A. Soffer and D. Aurbach, *J. Phys. Chem. C*, 2011, **115**, 16567–16573.
- 37 B. Shapira, E. Avraham and D. Aurbach, *Electrochim. Acta*, 2016, **220**, 285–295.
- 38 D. He, C. E. Wong, W. Tang, P. Kovalsky and T. David Waite, *Environ. Sci. Technol. Lett.*, 2016, **3**, 222–226.
- 39 R. Niu, H. Li, Y. Ma, L. He and J. Li, *Electrochim. Acta*, 2015, **176**, 755–762.
- 40 T. Yan, B. Xu, J. Zhang, L. Shi and D. Zhang, *RSC Adv.*, 2018, **8**, 2490–2497.
- 41 H. R. Park, J. Choi, S. Yang, S. J. Kwak, S. Il Jeon, M. H. Han and D. K. Kim, *RSC Adv.*, 2016, **6**, 69720–69727.
- 42 S. Daripa, V. K. Singh, O. Prakash, P. Maiti, B. K. Kuila and S. Das, *Nano-Struct. Nano-Objects*, 2020, **24**, 100531.
- 43 J. Yang, L. Zou and N. R. Choudhury, *Electrochim. Acta*, 2013, **91**, 11–19.
- 44 P. Liu, H. Wang, T. Yan, J. Zhang, L. Shi and D. Zhang, *J. Mater. Chem. A*, 2016, **4**, 5303–5313.
- 45 D. Ma, Y. Cai, Y. Wang, S. Xu, J. Wang and M. U. Khan, *ACS Appl. Mater. Interfaces*, 2019, **11**, 17617–17628.
- 46 B. H. Min, J. H. Choi and K. Y. Jung, *Electrochim. Acta*, 2018, **270**, 543–551.
- 47 Y. Algurainy and D. F. Call, *ACS ES&T Engg*, 2021, **2**, 129–139.
- 48 I. Cohen, E. Avraham, Y. Bouhadana, A. Soffer and D. Aurbach, *Electrochim. Acta*, 2015, **153**, 106–114.
- 49 D. Lu, W. Cai and Y. Wang, *Desalination*, 2017, **424**, 53–61.
- 50 A. Hemmatifar, D. I. Oyarzun, J. W. Palko, S. A. Hawks, M. Stadermann and J. G. Santiago, *Water Res.*, 2017, **122**, 387–397.
- 51 B. R. Puri, A. K. Balwara and R. S. Ilazra, *J. Indian Chem. Soc.*, 1967, **44**, 975–979.
- 52 B. R. Puri and P. L. Walker, *Chem. Phys. Carbon.*, Marcel Dekker, New York, 1970, pp. 191–282.
- 53 A. P. Terzyk, *J. Colloid Interface Sci.*, 2003, **268**, 301–329.
- 54 R. Xing, Y. Liu, Y. Wang, L. Chen, H. Wu, Y. Jiang, M. He and P. Wu, *Microporous Mesoporous Mater.*, 2007, **105**, 41–48.
- 55 M. Molina-Sabio, M. A. Muñecas-Vidal and F. Rodriguez-Reinoso, *Stud. Surf. Sci. Catal.*, 1991, **62**, 329–339.
- 56 J.-W. Shim, S.-J. Park and S.-K. Ryu, *Carbon*, 2001, **39**, 1635–1642.
- 57 A. Macías-García, M. A. Diaz-Diez, E. M. Cuerda-Correa, M. Olivares-Marin and J. Ganan-Gomez, *Appl. Surf. Sci.*, 2006, **252**, 5972–5975.
- 58 N. Holubowitch, A. Omosebi, X. Gao, J. Landon and K. Liu, *ChemElectroChem*, 2017, **4**, 2404–2413.
- 59 B. Pillay, *J. Electrochem. Soc.*, 1996, **143**, 1806.
- 60 Y. P. Wu, S. Fang, Y. Jiang and R. Holze, *J. Power Sources*, 2002, **108**, 245–249.
- 61 X. Zhang, K. Zuo, X. Zhang, C. Zhang and P. Liang, *Environ. Sci.: Water Res. Technol.*, 2020, **6**, 243–257.
- 62 J. Nordstrand and J. Dutta, *Desalination*, 2021, **500**, 114842.
- 63 S. Hand, J. S. Guest and R. D. Cusick, *Environ. Sci. Technol.*, 2019, **53**, 13353–13363.
- 64 M. Metzger, M. M. Besli, S. Kuppan, S. Hellstrom, S. Kim, E. Sebti, C. V. Subban and J. Christensen, *Energy Environ. Sci.*, 2020, **13**, 1544–1560.